Electronic Supplementary Material (ESI) for Inorganic Chemistry Frontiers.

# Experimental, DFT and Quantum Monte Carlo Studies of A Series of Peptide-based Metal-Organic Frameworks: Synthesis, Structures and Properties

**Gui-lin Zhuang,[a] Li Tan, [a]Wu-lin Chen,[ac] Jun Zheng,[b]Hong-zhou Yao,[a] Xing Zhong,[a]Jian-guo Wang*[a]**

[a]*Institute of Industrial Catalysis, College of Chemical Engineering, Zhejiang University of Technology, Hangzhou, People's Republic of China, 310032.*

*Fax: (+86)571-88871037 Tel: (+86)571-88871037*

*E-mail:* jgw@zjut.edu.cn

[b] *Center of Modern Experimental Technology, Anhui University, Hefei, People's Republic of China,230039.*

[c]*Zhejiang Engineering Design Co., Ltd. Hangzhou, People's Republic of China.*

## 1. Experimental Section: Synthesis, Crystallographic data and Measurement.

2, 5-piperazinedione-1, 4-diacetic acid was prepared based on our previous work[1]. Other reagents were of commercial origin without further purification. The C, H, and N element analyses were performed by use of a CE instruments EA 1110 elemental analyzer. The infrared spectra were measured on a Nicolet AVATAR FT-IR360 Spectrophotometer with pressed KBr pellets. The X-ray powder diffractometry (XRPD) study was performed on Panalytical X-Pert pro diffractometer with Cu-Ka radiation. TGA curves were prepared on a SDT Q600 Thermal Analyzer. Magnetic measurements were performed by a Quantum Design MPMS superconducting quantum interference device (SQUID).

**Synthesis of{[Mn(PODC)($H_2O$)$_2$]} ( 1 )** A mixture of 0.099 g $MnCl_2\cdot 4H_2O$ ( 0.5 mmol ) and 0.115 g $H_2$PODC ( 0.5 mmol ) were dissolved in water-N, N-Dimethylformamide (DMF) mixed solvent (10 mL, v/v= 1:1) and then under ultrasonic treatment for 10 min. The solution was subsequently sealed to 25 mL Teflon-lined Parr at 120 $^oC$ for 3 day and then cooled to room temprature at a rate of 5 $^oC\cdot h^{-1}$ . The white crystals were obtained with 36.5% yield ( based on $H_2$PODC). Anal. Calcd. ( Found ) for $C_8H_{12}N_2O_8Mn$ (1): C, 30.11(29.95); N, 8.78(9.08); H, 3.79(3.90). IR Spectra for 1 ( KBr, cm-1 ): 479(w), 658 (w), 807 (w), 965 (m), 1104 (w), 1178 (m), 1313 (w), 1353 (w), 1416 (w), 1494 (w), 1604 (s), 1624 (s), 2939 (w), 3359 (w).

**Synthesis of {[Fe(PODC)($H_2O$)$_2$]} ( 2 )** A mixture of 0.139 g $FeSO_4 \cdot 7H_2O$ ( 0.5 mmol ) and 0.115 g $H_2$PODC ( 0.5 mmol ) were added to water-ethanol mixed solvent (10 mL, v/v = 1:1). The pH value of solution was slowly adjusted to 4-5 by use of triethylamine. Subsequently, the mixture was sealed to 25 mL Teflon-lined Parr at 105 $^oC$ for six hours and then cooled to room temperature at a rate of 5 $^oC \cdot h^{-1}$. Colorless block crystals were obtained with 29.4% yield (based on $H_2$PODC). Anal. Calcd. (Found) for $C_8H_{12}N_2O_8Fe$ (2): C, 30.02(29.98); N, 8.75(8.62); H, 3.78(3.51). IR Spectra for **2** ( KBr, $cm^{-1}$): 429(w), 484(m), 586(w), 615(w), 671(w), 807(w), 861(w), 931(w), 969(m), 1105(w),1179(m), 1312(w), 1356(w), 1416(m), 1495(w), 1599(s), 1625(s), 2844(w), 2939 (w).

**Synthesis of {[Co(PODC)($H_2O$)$_2$]}( 3 )** 0.146 g Co(NO3)2·6H2O( 0.5 mmol ) and 0.115 g H2PODC ( 0.5 mmol ) were both added to water-ethanol mixed solvent (10 mL, v/v = 1:1). The pH of solution was slowly adjusted to 5–5.5 by use of triethylamine. Subsequently, the mixture was sealed to 25 mL Teflon-lined Parr at 135 $^oC$ for three days and then cooled to room temperature at a rate of 5 $^oC \cdot h^{-1}$. The pink crystals were obtained with 42.7% yield ( based on H2PODC ). Anal. Calcd. ( Found ) for $C_8H_{12}N_2O_8Co$ ( 3 ): C, 29.74 (29.01); N, 8.67( 8.04 ); H, 3.74( 3.98 ). IR Spectra for **3** ( KBr, $cm^{-1}$ ): 428 (w), 485 (m), 674 (w), 808 (w), 1106 (w),1179 (w), 1313 (w), 1356 (w), 1419 (m), 1495 (m), 1599 (s), 1625 (s), 2940 (w), 3350 (w).

**Synthesis of {[Cu(PODC)($H_2O$)$_2$]}( 4 ):** A mixture of 0.121 g $Cu(NO_3)_2 \cdot 3H_2O$(0.5 mmol) and 0.115 g $H_2$PODC (0.5 mmol) were added to water-DMF mixed solvent (10 mL, v/v= 1:1) and then further dissolved by ultrasonic treatment for 15 min. The solution was subsequently sealed to 25 mL Teflon-lined Parr at 105 $^oC$ for one day and then cooled to room temprature at a rate of 5 $^oC \cdot h^{-1}$ . The blue crystals were obtained with 30.3% yield ( based on $H_2$PODC ). Anal. Calcd. ( Found ) for $C_8H_{12}N_2O_8Cu$ (**4**): C, 29.31(28.99); N, 8.55(8.80); H, 3.69(4.01). IR

Spectra for **4** ( KBr, $cm^{-1}$ ): 440(w), 504(w), 582 (w), 655 (m), 722 (w), 808 (w), 904 (w), 941 (w), 967 (w), 1123 (s), 1193(s), 1321(m), 1342(w), 1389(s), 1428(s), 1495(w), 1565(s), 1659(s), 2928(w).

**Synthesis of {[$Ag_2$(PODC)]}( 5 ):** 0.017 g $AgNO_3$( 0.1 mmol ) was added to 0.023 g $H_2$PODC (0.1 mmol) were dissolved in 6 mL solvent (water-DMF = 1:1) and then was further exposed to ultrasonic for 3 h. The resulting cloudy solution was filtrated, and the colorless filtrate was kept for evaporation at room temperature for ten days until the white crystals were obtained with 32.4% yield (based on $H_2$PODC). Anal. Calcd. ( Found ) for $C_4H_4NO_3Ag$ (**5**): C, 21.65(20.98); N, 6.31(6.05); H, 1.82(2.20). IR Spectra for **5** (KBr, $cm^{-1}$): 490(w), 581 (w), 605(w), 705 (m), 805 (w), 910 (w), 959 (w), 1109 (w), 1184(w), 1262 (w), 1289 (m), 1352 (w), 1382 (s), 1497(m), 1599 (s), 1654 (s), 2940 (w), 2983 (w)

**Synthesis of {[Pb(PODC)($H_2O$)] ($H_2O$)$_4$}( 6 ):** A mixture of 0.165 g $Pb(NO_3)_2$( 0.5 mmol ) and 0.115 g $H_2$PODC (0.5 mmol) were dissolved in 10 mL solvent (water: DMF = 1:1) while stirring for 10 min. Then the mixture was subsequently sealed in a 15 mL glass vessel under ultrasonic irradiation for 3 h. The resulting cloudy solution was filtrated, and the colorless filtrate was kept for evaporation at room temperature for one week until the white crystals were obtained with 42.1% yield (based on $H_2$PODC). Anal. Calcd. ( Found ) for $C_8H_{18}N_2O11Pb$ ( **6** ): C, 18.29(18.55); N, 5.33(5.18); H, 3.45(3.77). IR Spectra for **6** (KBr, $cm^{-1}$): 490(w), 575(w), 710(m), 781(m), 926(w), 962(m), 1192(w), 1300(w), 1350(m), 1388(m), 1428(w), 1490(w), 1570(s), 1637(s), 2830(w), 2930(w).

Single crystals having suitable dimensions for compounds **1-6** were used for data collection using a CrysAlis CCD diffractometer ( Xcalibur, Eos, Gemini ultra ) at298 K equipped with Enhance (Mo) X-ray Source ($\lambda$ = 0.71073 Å). Integration and cell refinement was carried out using CrysAlis RED. The absorption correction was performed by multi-scan method using SCALE3 ABSPACK scaling algorithm. All Corrections were made for Lorentz and polarization effects. The molecular structures were solved by direct methods (SHELXL-86/SHELXL-

97)[2] and refinement by full-matrix least-squares on $F^2$ (SHELXS-97). Crystal data and selective bond length and bond angle of compounds **1-6** are given in Table S1 and S2.

Table **S1** Crystal data and details of data collection and refinement for compounds **1**–**6**

| **Compound** | **1** | **2** | **3** | **4** | **5** | **6** |
|---|---|---|---|---|---|---|
| Formula | $C_8H_{12}N_2O_8Mn$ | $C_8H_{12}N_2O_8Fe$ | $C_8H_{12}N_2O_8Co$ | $C_8H_{12}N_2O_8Cu$ | $C_4H_4NO_3Ag$ | $C_8H_{18}N_2O_{11}Pb$ |
| *Mr* | 319.14 | 320.05 | 323.13 | 327.74 | 221.95 | 525.43 |
| Crystal system | Monoclinic | Monoclinic | Monoclinic | Monoclinic | Monoclinic | Triclinic |
| Space group | *P*2(1)/c | *P*2(1)/c | *P*2(1)/c | *C*2/c | *P*2(1)/n | *P*-1 |
| *a*/Å | 7.8275(3) | 7.7479(6) | 7.7384(3) | 20.5479(8) | 4.9863(2) | 6.9587(3) |
| *b*/Å | 9.4883(3) | 9.4157(6) | 9.3942(4) | 4.65730(10) | 11.9186(5) | 10.0635(5) |
| *c*/Å | 7.6738(3) | 7.5296(5) | 7.5455(3) | 13.9774(6) | 8.8591(3) | 11.2625(5) |
| *α*/deg | 90 | 90 | 90 | 90 | 90 | 79.014(4) |
| *β*/deg | 108.524(4) | 108.562(8) | 108.574(4) | 124.401(6) | 98.548(4) | 84.469(4) |
| *γ*/deg | 90 | 90.00 | 90 | 90 | 90 | 88.510(4) |
| $V/Å^3$ | 540.40(3) | 520.72(6) | 519.96(4) | 1103.66(7) | 520.65(3) | 770.62(6) |
| *Z* | 2 | 2 | 2 | 4 | 4 | 2 |
| $D_c$/g cm$^{-3}$ | 1.961 | 2.041 | 2.064 | 1.972 | 2.832 | 2.264 |
| *μ*/mm$^{-1}$ | 1.265 | 1.494 | 1.696 | 2.022 | 3.784 | 11.004 |
| Data/params | 1060/96 | 1017/96 | 1192/97 | 1080/96 | 1015/83 | 3029/199 |
| *θ*/deg | 3.49-26.00 | 3.52-25.99 | 3.52-28.98 | 2.94-25.99 | 3.42-25.98 | 3.02-26.00 |
| Obs reflns | 991 | 958 | 1128 | 986 | 953 | 2880 |
| Goof on $F^2$ | 1.104 | 1.079 | 1.128 | 1.150 | 1.125 | 1.032 |
| $R_1[I>2\sigma(I)]^a$ | 0.0275 | 0.0213 | 0.0213 | 0.0225 | 0.0508 | 0.0238 |
| $wR_2$(All data)$^b$ | 0.0828 | 0.0568 | 0.0601 | 0.0562 | 0.1385 | 0.0601 |

$^aR_1 = \Sigma||F_O| - |F_C||/\Sigma|F_O|$  $^bwR_2 = \{\Sigma[w(F_O^2 - F_C^2)^2]/\Sigma[w(F_O^2)^2]\}^{1/2}$

**Table S2** Selected bond lengths (Å) and angles (°) for **1** – **6**.

**Compound1**

| | | | | | | | |
|---|---|---|---|---|---|---|---|
| Mn1-O2$^{i}$ | 2.1407(11) | Mn1-O3 | 2.1511(11) | Mn1-O1W | 2.2122(16) | | |
| O2$^{i}$-Mn1-O2$^{ii}$ | 180.00(6) | O2$^{i}$-Mn1-O3 | 87.13(5) | O2$^{ii}$-Mn1-O3 | 92.87(5) | O2$^{i}$-Mn1-O1W | 89.57(6) |
| O2$^{ii}$-Mn1-O1W | 90.43(6) | O3-Mn1-O1W | 86.48(5) | O3$^{iii}$-Mn1-O1W | 93.52(5) | | |

Symmetry codes: (i) -x+2,y-1/2,-z+1/2;(ii) x,-y+5/2,z-1/2;(iii) -x+2,-y+2,-z

| | | | | | | | |
|---|---|---|---|---|---|---|---|
| **Compound2** | | | | | | | |
| Fe1-O3$^{i}$ | 2.0689(11) | Fe1-O2$^{ii}$ | 2.1385(10) | Fe1-O1W | 2.1501(13) | | |
| O3$^{i}$ -Fe1-O3 | 180.00(6) | O3$^{i}$ -Fe1-O2$^{ii}$ | 86.04(4) | O3-Fe1-O2$^{ii}$ | 93.96(4) | O3-Fe1-O2$^{iii}$ | 86.04(4) |
| O3$^{i}$ -Fe1-O1W | 90.10(5) | O3-Fe1-O1W | 89.90(5) | O2$^{ii}$-Fe1-O1W | 94.98(4) | O2$^{iii}$-Fe1-O1W | 85.02(4) |
| Symmetry codes:(i) #1 -x+2,-y+2,-z;(ii) x,-y+5/2,z-1/2; (iii) -x+2,y-1/2,-z+1/2 | | | | | | | |
| **Compound 3** | | | | | | | |
| Co1-O2$^{i}$ | 2.0741(11) | Co1-O3 | 2.0908(11) | Co1-O1W | 2.1092(14) | | |
| O2$^{i}$ -Co1-O2#2 | 180.00(6) | O2$^{i}$-Co1-O3$^{iii}$ | 87.09(5) | O2$^{ii}$-Co1-O3$^{iii}$ | 92.91(5) | O2$^{i}$-Co1-O1W | 89.98(5) |
| O2$^{ii}$ -Co1-O1W | 90.02(5) | O3$^{iii}$-Co1-O1W | 93.72(5) | O3-Co1-O1W | 86.28(5) | | |
| Symmetry codes:(i) x,-y+3/2,z-1/2; (ii)-x+1,y-1/2,-z+1/2; (iii)-x+1,-y+1,-z | | | | | | | |
| **Compound 4** | | | | | | | |
| Cu1-O3 | 1.9501(14) | Cu1-O1W | 1.9573(15) | | | | |
| O3-Cu1-O3$^{i}$ | 180.00(7) | O3-Cu1-O1W | 88.17(7) | O3$^{i}$-Cu1-O1W | 91.83(7) | | |
| Symmetry codes:(i) -x+1/2,-y-3/2,-z-1 | | | | | | | |
| **Compound 5** | | | | | | | |
| Ag1-O2$^{i}$ | 2.184(4) | Ag1-O3 | 2.245(4) | Ag1-O1$^{ii}$ | 2.558(4) | Ag1-Ag1$^{i}$ | 2.7918(9) |
| Ag1-Ag1$^{iii}$ | 2.9348(8) | | | | | | |
| O2$^{i}$ -Ag1-O3 | 160.01(14) | O2$^{i}$ -Ag1-O1$^{ii}$ | 111.49(14) | O3-Ag1-O1$^{ii}$ | 78.67(14) | O2$^{i}$-Ag1-Ag1$^{i}$ | 86.52(10) |
| O3-Ag1-Ag1$^{i}$ | 77.97(10) | O1$^{ii}$-Ag1-Ag1$^{i}$ | 151.03(9) | O2$^{i}$-Ag1-Ag1$^{iii}$ | 136.70(10) | O3-Ag1-Ag1$^{i}$ | 63.16(10) |
| O1$^{ii}$-Ag1-Ag1$^{iii}$ | 60.83(9) | Ag1$^{i}$-Ag1-Ag1$^{iii}$ | 121.07(3) | | | | |
| Symmetry codes:(i) -x+1,-y+2,-z ; (ii) -x+1/2,y-1/2,-z+1/2; (iii) -x,-y+2,-z | | | | | | | |
| **Compound 6** | | | | | | | |
| Pb1-O6$^{i}$ | 2.478(2) | Pb1-O3 | 2.487(2) | Pb1-O4 | 2.657(3) | Pb1-O3$^{ii}$ | 2.659(2) |
| Pb1-O2 | 2.691(3) | | | | | | |
| O6$^{i}$-Pb1-O3 | 78.73(8) | O6$^{i}$-Pb1-O4 | 78.17(8) | O3-Pb1-O4 | 123.77(8) | O6$^{i}$-Pb1-O3$^{ii}$ | 70.91(8) |
| O3-Pb1-O3$^{ii}$ | 63.29(9) | O4-Pb1-O3$^{ii}$ | 146.22(7) | O3-Pb1-O2 | 50.15(7) | O4-Pb1-O2 | 75.15(8) |
| O3$^{ii}$-Pb1-O2 | 110.31(7) | | | | | | |
| Symmetry codes:(i)x-1,y,z; (ii)-x+1,-y+1,-z+1 | | | | | | | |

## 2. Detail of DFT calculation

Geometry optimization, electronic structure and optical properties were performed by using the projector-augmented wave ( PAW ) method of Blöchl[3], as implemented in the ab initio VASP program[4]. PAW method can combine the accuracy of augmented plane-wave methods with the efficiency of the pseudopotential approach. The generalized gradient approximation ( GGA ) with Perdew Burke Ernzerhof (PBE)[5] formalism was used to describe the exchange-correlation (XC) effects. The 4*d* and 5*s* electrons of Ag, 3*d* and 4*s* electrons of Mn and Cu, 2*s* and 2*p* electrons of C, N and O, and 1*s* electrons of H were explicitly treated as valence electrons. The electron wave function is expanded in plane waves up to a cutoff energy of 500 eV for **1**, 1050 eV for **5**. For the Brillouin zone integration, the Γ centered 3×3×4 grids for **1**, 6×6×2 grids for **4** and 9×3×6 grids for **5** were adopted. One non-local correlation vdW-DF based on opt88 functional was applied to correct the dispersion interaction. In the optical calculation of **5**, 408 bands were used to calculate dielectric function and a good convergence was obtained. Meanwhile, GGA+U algorithm[7] was used to correct the strongly correlated interaction in 3*d* electrons of Mn and Cu, and 4*d* electrons of Ag. The effective Hubbard $U_{\mathrm{eff}}$ values were identified by linear response method( see following details ). The optimization convergence in energy and force was set to $1.0\times10^{-5}$ eV and 2.0× 10-3 eV/Å, and the SCF convergence was set to $1.0\times10^{-6}$. Band structure and Partial Density of State (PDOS) were also identified. Frontier molecular orbits analysis at Gamma point was also plot. For the optimized geometry of VASP, frontier orbital analysis of **5** was carried out by using DMol3 program[8], with the functional of GGA-PBE[5] and DNP basic set[8a]. For **1** and **4**, spin magnetic moment $M = N(\uparrow) - N(\downarrow)$ is the difference between the number of spin-up and spin-down electrons, which can be obtained by integrating the corresponding spin-projected densities of states up to the Fermi level.

### The process of Geometry optimization

In this study, we choose the X-Ray experimental data as the initial geometry. The optimized process has two steps: Firstly, under the constraints of no-hydrogen atoms, all of hydrogen atoms were optimized; Secondly, all the atoms were fully relaxed at the optimized geometry. With the constraints of crystal parameters, the optimized local-stable configuration is in good agreement with that of X-ray analysis.

### $U_{\mathrm{eff}}$ of compounds 1, 4 and 5.

The $U_{\mathrm{eff}}$ of compound **1,** **4** and **5** was calculated by PWSCF[9] package using the linear response approach introduced by Cococcioni et.al[10]. In this calculation, we used the projector augmented wave ( PAW ) method with Perdew, Burke and Ernzerhof (

PBE ) exchange-correlation functional. Vanderbilt ultrasoft pseudopotentials[11] with the plane-wave energy cutoff of 35 Ryd were adopted. The 4×3×2 Monkhorst-Pack grid was employed in the sampling of Brillouin zone. 1×1×1 supercells of **1, 4** and **5** were adopted. By invariant formulation, the total energy of DFT+U can be described as follow:

$$E_{DFT+U}[n(r)] = E_{DFT}[n(r)] + E_U[\{n_{mm'}^{I\sigma}\}]$$

Where, $E_{\mathrm{DFT}}$ is a total energy from noninteraction Kohn-Sham algorithm; $E_{\mathrm{U}}$ is Hubbard correction.

Furthermore, if neglecting higher-multipolar terms of Coulomb interaction, $E_{\mathrm{U}}$ is written as:

$$E_U[\{n_{mm'}^{I\sigma}\}] = \frac{U-J}{2}\sum_{I,\sigma} Tr[n^{I\sigma}(1-n^{I\sigma})] = \frac{U_{eff}}{2}\sum_{I,\sigma} Tr[n^{I\sigma}(1-n^{I\sigma})]$$

By linear-response approach U method, the linear response function is defined as

$$\chi = \frac{\partial n}{\partial \alpha}$$

In this method, the interacting ($\chi$) and noninteractiong density response functions with respect to localized perturbations were firstly calculated. Thus U can be obtained by following formula:

$$U_{eff} = \chi^{-1} - \chi_0^{-1}$$

By changing the rigid potential shifts $\alpha$, we obtain the bare and self-consistent occupation regression response functions. The interacting ($\chi$) and the noninteracting ($\chi_0$) are the slopes of bare and self-consistent regression response functions, respectively. Therefore, the obtained $U_{eff}$ are 6.01 eV for **1**, 1.67 eV for **4** and 6.52 eV for **5**, as shown in Fig.S1.

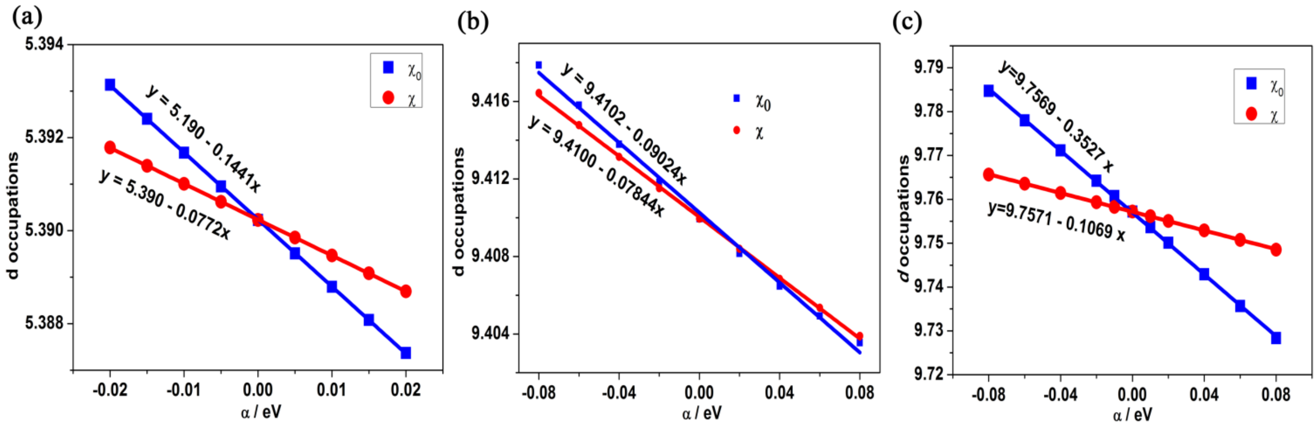

Figure S1 interacting ($\chi$) and noninteracting density response functions of **1(a), 4(b)** and **5(c)**.

## 3. Quantum Monte Carlo Fitting Details

**Algorithm of our fitting Program**: The quantum Monte Carlo calculations were performed by our fitting program, where we call LOOP module of ALPS[12]and utilize four parameters ($J$, $g$, $zJ$ and $TIP$ ) to further fit the experimental result by use of exhaustive-iterative method. The corresponding formulas were shown in Eq(1)-Eq(4). The running procedure of our program is presented in the Figure S2. In the beginning, the range of four parameters ( $J$, $g$, $TIP$, $zJ$ ) were respectively set to that: [$J_1$: $J_2$], [$g_1$: $g_2$], [$TIP_1$: $TIP_2$], [$zJ_1$: $zJ_2$], and the step sizes were set to $\Delta J$, $\Delta g$, $\Delta TIP$ and $\Delta zJ$. Until the running is over, the best parameters ($R_b$, $J_b$, $g_b$, $TIP_b$, $zJ_b$) were obtained.

$$\chi_u = \frac{1}{NT}\left\langle\left(\sum_{i=1}^{N} S_i^z\right)^2\right\rangle \qquad \text{Eq(1)}$$

where uniform magnetic susceptibility $\chi_u$ is dimensionless.

Convert uniform magnetic susceptibility to $\chi_T$ (cm$^3$mol$^{-1}$)

$$\chi_T(cm^3mol^{-1}) = Ag^2\chi_u \qquad \text{Eq(2)}$$

where $g$ is Landég-factor and $A$ is unit constant.

Import $zJ$ and $TIP$ factor to $\chi_T$ , as bellows:

$$\chi_T^{'}(cm^3mol^{-1}) = \frac{(\chi_T + TIP)}{1 + \frac{zJ(\chi_T + TIP)}{0.1303g^2}} \qquad \text{Eq(3)}$$

The reliability factor *R* is obtained by

$$R = \frac{\sum(\chi_T^{'}T - \chi_{obs}T)^2}{\sum(\chi_{obs}T)^2} \qquad \text{Eq(4)}$$

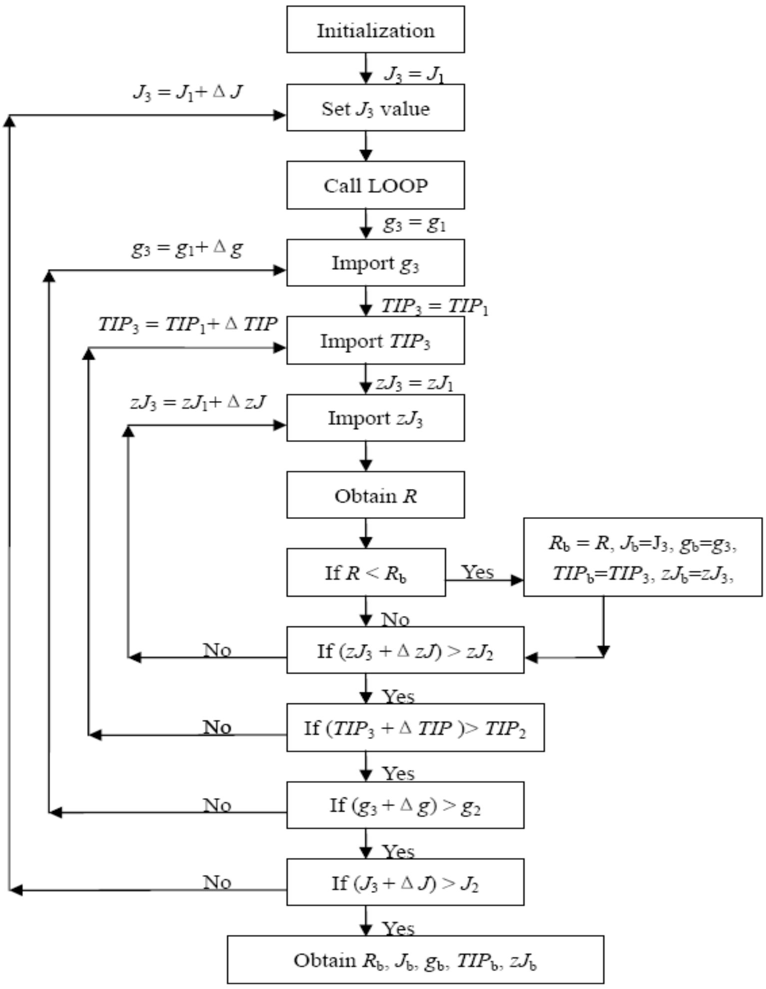

Figure S2 the procedure of our program.

**Parameters of QMC in 1 and 4**: For each site, 2×10$^6$ Monte Carlo steps and 2× 10$^5$ Monte Carlo sweeps for thermalization were performed. The sample is 25 × 25 spins for **1**, 500 spins for **4**, which is large enough to prevent any finite size effects. Moreover, periodic boundary conditions (PBC) were applied in order to avoid perturbation from the edge of the sample and speed up convergence toward the infinite lattice limit.

## 4. Coordination modes of $H_2$PODC ligand

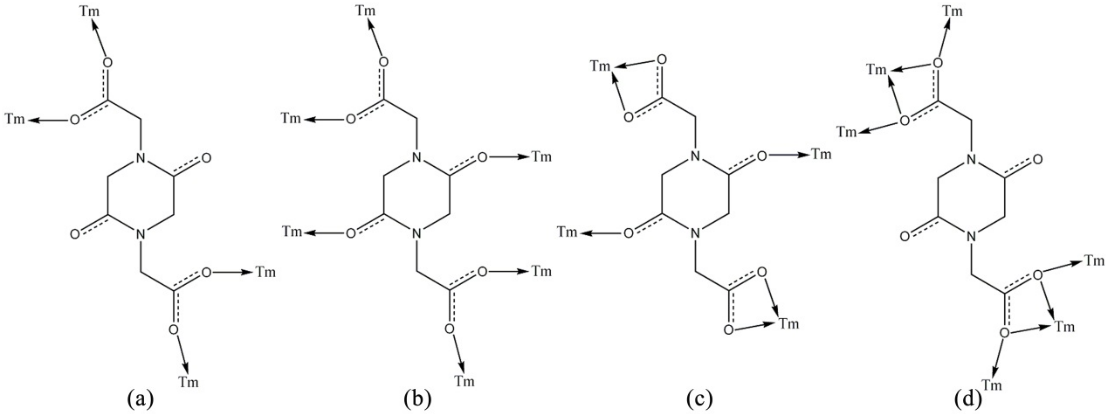

Figure S3 four coordination modes of $H_2PODC$ ligand.

## 5. Space filling view of 6

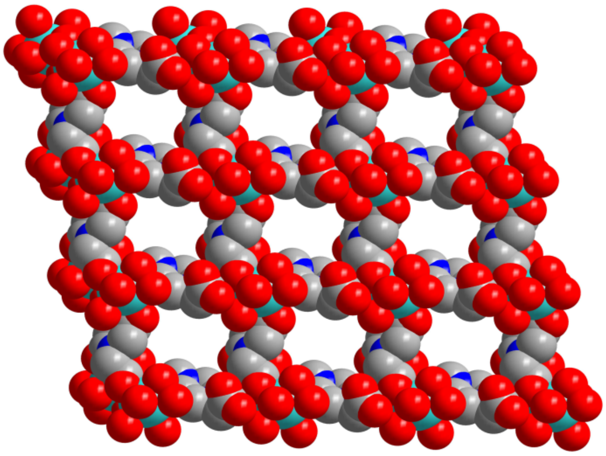

Figure S4 space filling view of **6**.

## 6. Figure of TGA for compounds 1-6

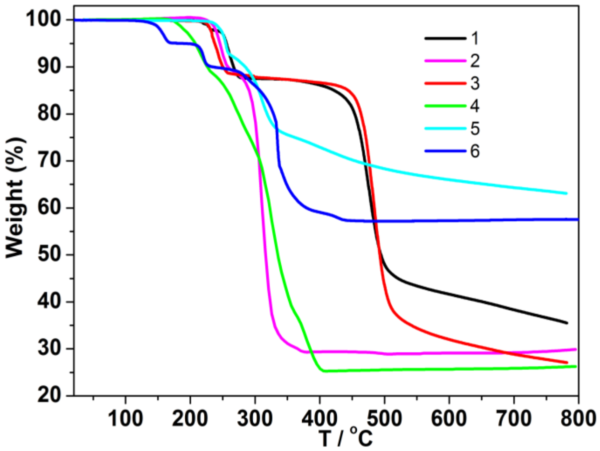

Figure S5 TGA curves for compounds **1-6** with the range of room temperature and 800 °C.

Thermogravimetric analysis (TGA) studies were also performed in an air atmosphere at a heating rate of 10 °C/min$^{-1}$ for compounds **1-6,** as shown in Fig. S5. For the case of **1-3**, the first weight loss ( 11.67% for 1, 11.22% for **2** and 11.40% for **3**) were found at 250 °C, which suggests removal of two aqua ligands ( theoretically calcd 11.3% for **1**, 11.24% for **2** and 11.14% for **3** ). Once losing the coordinated water molecules, the structure of 1-3 began to decompose. **4** keeps stable until 164 °C and rapidly decomposes with the removal of two aqua ligands. The residual product of 25.30% is CuO ( theoretically calcd 24.40% ). Similarly, when the temperature is up to 228 °C, the framework of **5** begins to collapse, due to the loss of two aqua ligands. In **6**, the first weight loss ( *c.a.* 5.00%) at 123 °C hints two guest water molecules are removed with the theoretical value of 6.80%. At this time, the whole framework keeps stable. Until 223 °C, the third guest water molecule (*c.a.* 9.98% ) was removed, which is also in line with the theoretical value of 10.27%. Subsequently, with the loss of aqua ligand, the whole structure rapidly collapses.

## 7. $\chi_m^{-1}$ *vs* T plot of compounds 1-3

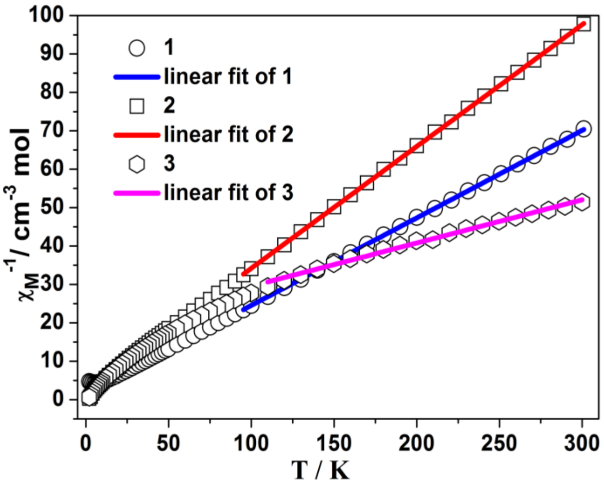

**Figure S6** $\chi_m^{-1}$ *vs* T plots of **1**(○), **2**(□) and **3**(◊) and linear fitting over the range of 100K-300K of **1**(blue solid line), **2**(red solid line), **3**(pink solid line).

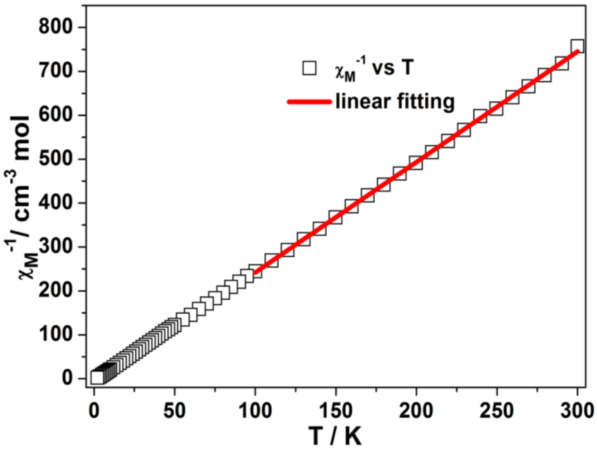

**Figure S7** $\chi_m^{-1}$ *vs* T plots of **4** and linear fitting over the range of 100K-300K of **4** ( red solid line )

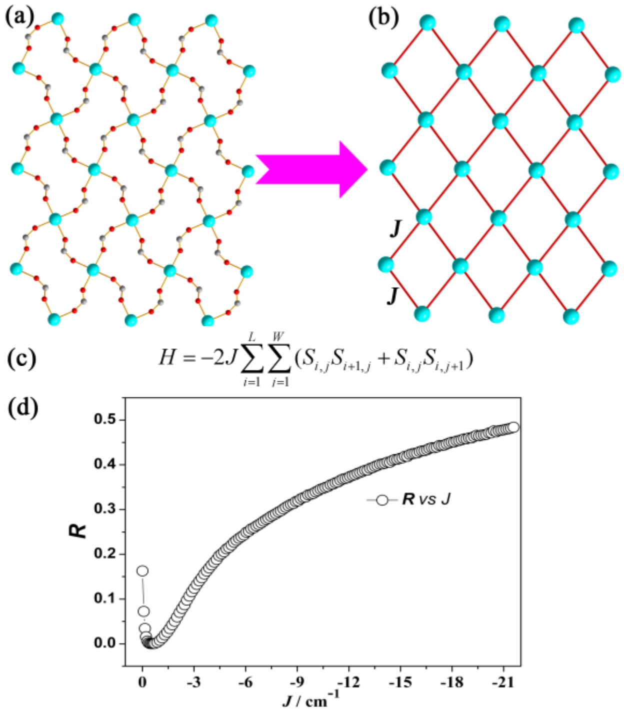

(c) $$H = -2J\sum_{i=1}^{L}\sum_{j=1}^{W}(S_{i,j}S_{i+1,j} + S_{i,j}S_{i,j+1})$$

**Figure S8** The sketch of $Mn^{2+}$ distribution in **1** (a-b)**;**.Hamilton operator of **1**(c); plot of *R vs J*(d).

## 8. IR spetra of compounds 1-6

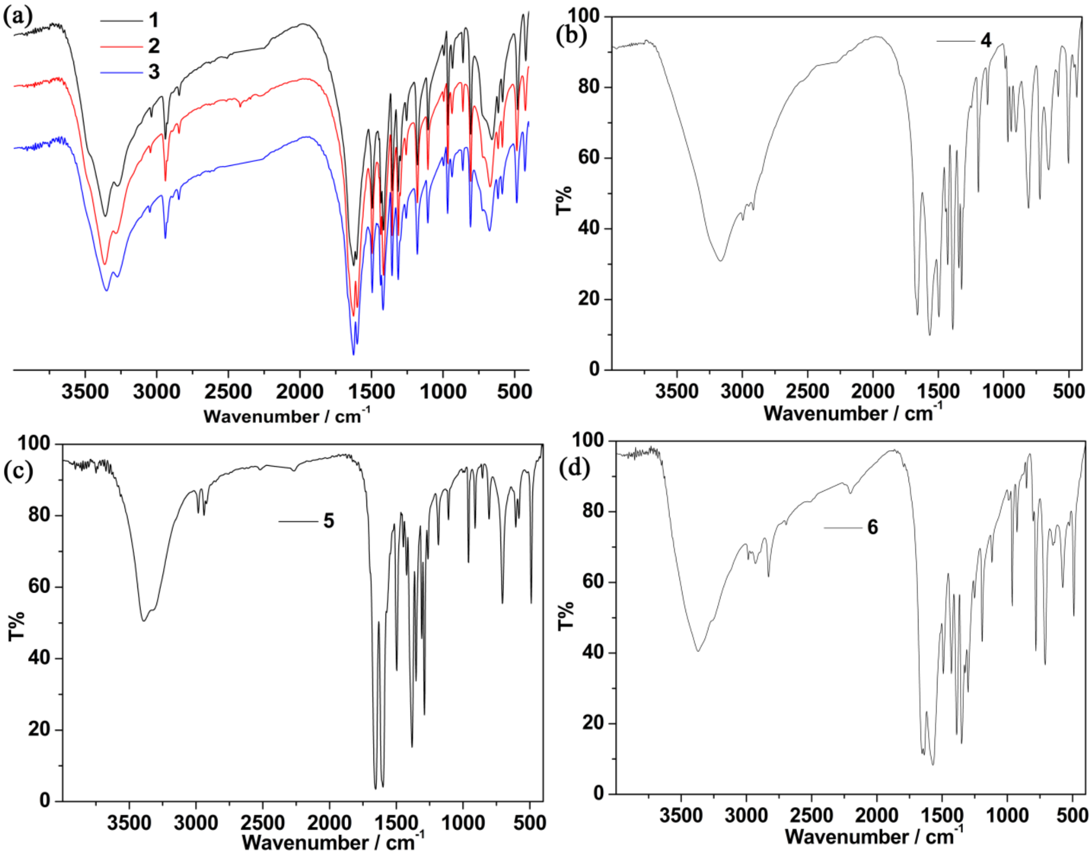

Figure S9 IR spectra of compounds **1-6**.

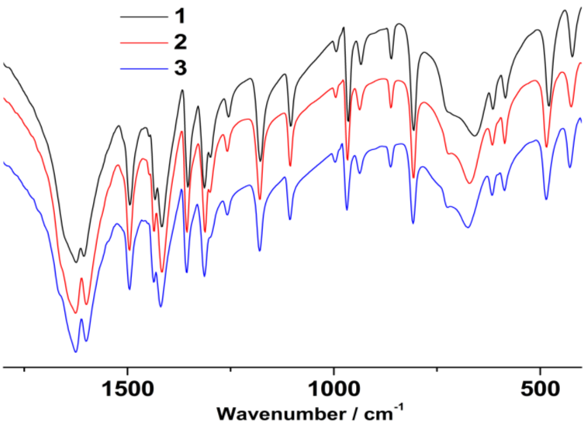

Figure S10 IR of compound **1-3** with the range from 400 cm$^{-1}$ to 1800 cm$^{-1}$.

## 9. XRD Curve of compounds 1-5

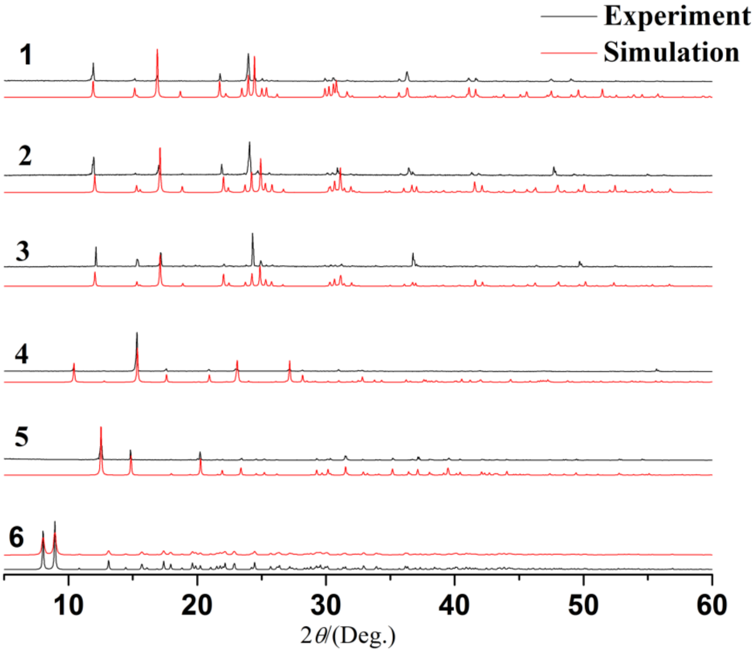

Fig. S11 XRD curve of compounds **1-6**

## 10. UV-vis theoretical curve of compound 5

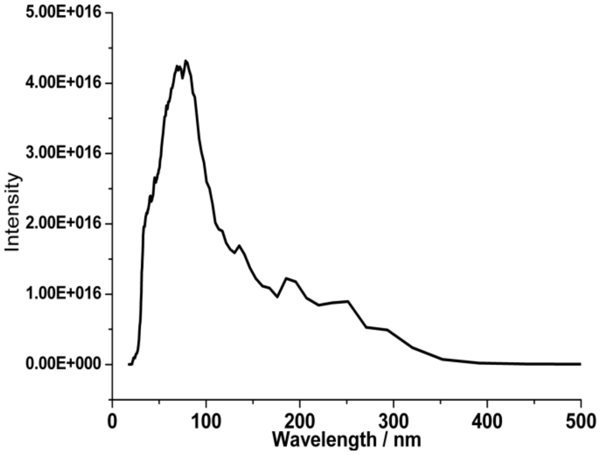

Fig. S12 UV-vis theoretical curve of compounds **5**

**Reference:**

[1] X. J. Kong, G. L. Zhuang, Y. P. Ren, L. S. Long, R. B. Huang, L. S. Zheng, *Dalton Trans*, 2009, 1707.

[2] G. M. Sheldrick, *Acta Cryst*, 2008, **A64**, 112.

[3] P. E. Blöchl, *Phys. Rev. B*, 1994, **50**, 17953.

[4] G. Kresse, J. Hafner, *Phys. Rev. B*, 1993, **48**, 13115.

[5] J. P. Perdew, K. Burke, M. Ernzerhof, *Phys. Rev. Lett*, 1996, **77**, 3865.

[6] M. Dion, H. Rydberg, E. Schröder, D. C. Langreth, B. I. Lundqvist, *Phys. Rev. Lett*, 2004, **92**, 246401.

[7] V. I. Anisimov, I. V. Solovyev, M. A. Korotin, *Phys. Rev. B*, 1993, **48**, 16929.

[8] (a) B. J. Delley, *Chem. Phys*, 1990, **92**, 508. (b) B. J. Delley, *Chem. Phys*,2000, **113**, 7756. (c) B. J. Delley, *Chem. Phys*, 1991, **94**, 7245.

[9] P. Giannozzi, S. Baroni, N. Bonini, M. Calandra, R. Car, et.al. *J.Phys.:Condens.Matter*, 2009, 21, 395502.

[10] M.Cococcioni, S.de Gironcoli, *Phys. Rev. B* 2005, **71**, 035105.

[11] D.Vanderbilt, *Phys. Rev. B,* 1990, **41**, 7892.

[12] B. Bauer, L.D. Carr, H. G. Evertz, A. Feiguin, *J. Stat. Mech*, 2011, P05001.